Upconversion at Solid/Liquid Interfaces using Perovskite Single Crystal Triplet Sensitizers

Gregory Moller,[1,2,#] Colette M. Sullivan,[1,#] Andrew P. Cantrell,[1] Masoud Mardani,[2,3] Alexander S. Bieber,[1] Theo Siegrist,[2,4,] Lea Nienhaus[1,*]*

[1] Department of Chemistry and Biochemistry, Florida State University, Tallahassee, FL 32306, USA

[2] National High Magnetic Field Laboratory, Tallahassee, FL 32310, USA

[3] Department of Physics, Florida State University, Tallahassee, FL 32306, USA

[4] FAMU-FSU College of Engineering, Tallahassee, FL 32310, USA

[#]equal contribution

*Corresponding Author: siegrist@magnet.fsu.edu and lnienhaus@fsu.edu

ABSTRACT

Perovskite-sensitized photon upconversion (UC) has the potential to improve a wide range of technologies including photocatalysis and photovoltaics, by converting two low energy photons into a single photon of higher energy.[1–4] To date, perovskite-sensitized UC has been studied using nanocrystals in solution and solid-state thin film bilayers using polycrystalline perovskite films. While efficient UC has been achieved in thin film bilayers, surface inhomogeneities and defects due to individual perovskite crystal grains and grain boundaries may limit the overall performance. However, one of the main issues in solid-state UC is a limited number of viable triplet annihilators in solid-state due to unfavorable intermolecular interactions and competing relaxation pathways. Here, we investigate the properties of a mixed cation methylammonium formamidinium lead triiodide perovskite single crystals using x-ray diffraction and optical spectroscopy and its subsequent incorporation and performance as a triplet sensitizer for triplet-triplet annihilation in solution-based rubrene. With the hybrid solid-state/solution approach presented here, a wide number of potential annihilators can rapidly be screened. In addition, the higher surface homogeneity and orders of magnitude lower defect densities and higher stability of perovskite single crystals allow for potential improvements to interfacial charge transfer processes and increases in UC performance due to reduced carrier trapping.

INTRODUCTION

Since their discovery in 1839, perovskite materials have evolved into an incredibly broad class of materials with a general formula ABX_3.[5] Metal halide perovskites are an emerging class of semiconductor materials with applications including radiation detection,[6] light emitting diodes,[7] the active layer in photovoltaics,[8] and as triplet sensitizers in photon upconversion (UC).[9] The first use of a metal halide perovskite as the light absorbing material in a solar cell was in a study done in 2009 by Kojima *et. al.,* which reported a power conversion efficiency of 3.81%.[10] Since then, the record efficiency for single junction perovskite solar cells has skyrocketed over 25% in 2021, rivaling commercial single junction silicon cells.[11,12] Their rapid increase in performance can be attributed to a combination of their high defect tolerance,[13] long carrier diffusion lengths,[14] and tunable optical properties across the visible and near-infrared spectral region.[15] In the general ABX_3 formula, the A-site is a monovalent cation (here: methylammonium (MA) and formamidinium (FA), B is a divalent Pb^{2+} cation, and X is a halide anion. Both single crystals and polycrystalline thin films have been widely studied,[16] where single crystals generally exhibit lower defect densities and long carrier lifetimes and diffusion lengths and a lower number of grain boundaries.[14,17]

To date, bulk perovskite-sensitized triplet-triplet annihilation (TTA) UC has primarily been studied within solution processed polycrystalline bilayer thin films composed of a bulk lead halide perovskite sensitizer coupled with a thin film of an annihilator such as rubrene, 1-chloro-9,10-bis(phenylethynyl)anthracene or naphtho[2,3-a]pyrene.[9,18–20] TTA-UC is a spin-allowed process in which an interaction between two spin-triplets yields a singlet excited state and ground state.[1,4,21] Since direct optical excitation to the triplet excited state is a spin-forbidden process, triplet sensitizers are commonly utilized to efficiently populate the annihilator triplet state.[3,22] In the case of bulk perovskite sensitizers, recombination of free carriers results in the bound triplet state on the organic molecule,[23,24] while in the case of (perovskite) nanocrystal sensitizers, often, the energy packet is transferred in form of a bound exciton.[25–28]

Solution processing of the underlying perovskite film and the subsequent organic film fabrication results in a wide variety of environments which adds a level of complexity when building an understanding of the

upconversion mechanism and nanoscale charge transfer processes.[29] To improve the overall understanding of charge transfer at the interface between the perovskite and the annihilator, and the unclear role of surface and bulk defects limiting charge extraction at the interface,[29,30] we investigate perovskite single crystals (SCs) as triplet sensitizers. In contrast to polycrystalline films, SC perovskites have fewer grain boundaries and discontinuities or defects that may affect the optical and electronic performance of the devices, most of which are shielded by the high dielectric constant.[31] Previous studies have shown lower trap-state densities and longer diffusion lengths and increased carrier mobility for SCs compared to polycrystalline films,[14] suggesting their potential to act as better sensitizers for TTA-UC, since more charges may reach the interface within their lifetime. Their single crystalline structure and lower defect density as compared to polycrystalline perovskite thin films provide a simplified surface for studying the fundamental nanoscale charge transfer processes between perovskite sensitizers and annihilator molecules.[29]

While previous thin film perovskite-sensitized UC was performed in a solid-state bilayer, here, we opt for a hybrid solid-state sensitizer/solution-phase annihilator approach to be able to directly compare different SCs without having additional complications from different local molecular environments in rubrene.[32–34] While this hybrid approach is not viable for subsequent photovoltaic applications, its successful implementation indicates the strong promise of solid-state perovskite sensitizers in heterogeneous photocatalytic applications such as solution-based triplet-driven cross-coupling reactions.[35–37]

RESULTS AND DISCUSSION

Perovskite single crystals based on a 1:1 precursor ratio of methylammonium (MA) and formamidinium (FA) ($MA_{0.5}FA_{0.5}PbI_3$) are grown based on the inverse temperature crystallization (ITC) method adapted from Saidaminov *et al*.[38] ITC is based on a property unique to perovskites, which was initially attributed to an inverse relationship between solubility and temperature. In contrast to most solutes where temperature increases commonly result in an increase in solubility, the solubility of the perovskite precursors decreases

with increasing temperature in DMF or γ-butyrolactone (GBL).[38] In ITC, as the temperature of a concentrated precursor solution is increased above 100 °C, the solubility decreases and perovskite SCs will begin to grow, with typical growth time varying between 30 minutes to three hours. A study on the growth mechanism done by Nayak *et al.* found that the crystal growth was caused primarily by solvent decomposition at high temperatures, increasing the pH of the solution, leading to the disintegration of colloids containing undissolved precursor resulting in a supersaturated solution.[39] Here, GBL degrades to γ-hydroxybutyrate (GHB), supplying the H^+ needed to break up the colloidal clusters of undissolved PbI_2.

Figure 1a outlines the general process of ITC: the precursor solution was heated under ambient conditions until the perovskite SCs begin to form. $MA_{0.5}FA_{0.5}PbI_3$ SCs were successfully grown using a solvent-assisted ITC method where stock solutions of 1 M $MAPbI_3$ and $FAPbI_3$ were prepared in GBL. Since $MAPbI_3$ did not fully dissolve in GBL, the stock solution volume was diluted with acetonitrile (ACN) to fully dissolve the $MAPbI_3$ precursor, which should also help to form the desired n-type surface doping for efficient charge extraction.[29] Equal parts of $MAPbI_3$ and $FAPbI_3$ precursors were combined into a final $MA_{0.5}FA_{0.5}PbI_3$ growth solution that was heated to 120 °C, at which point small crystals began to form and were subsequently harvested and stored in a nitrogen environment until further use (Figure 1a).

The crystal structures of the resulting $MA_{0.5}FA_{0.5}PbI_3$ SCs were investigated using an Oxford Diffraction Xcalibur-2 CCD single crystal diffractometer. At room temperature, the x-ray data showed the expected cubic perovskite substructure, with lattice parameter a = 6.3224(5) Å at 295 K (Figure 1b). Previous results have shown that $MAPbI_3$ SCs grown *via* the ITC method exhibit a cubic-to-tetragonal phase transition at 330 K due to the elevated temperatures associated with the synthetic procedure.[40] Twinning crystallographic effects, thus, can stem from the loss of symmetry elements during this transition.[16,40] No tetragonal superstructure reflections are observed at room temperature for the mixed cation $MA_{0.5}FA_{0.5}PbI_3$ grown here, indicating that it is still present in a cubic crystal structure at this temperature, likely a result of the mixed cation composition. Temperature-dependent x-ray diffraction measurements indicate an apparent doubling along all axes below the phase transition temperature of 257 K, consistent with ordering of the

FA/MA molecules in a multiply twinned arrangement with an apparent cubic unit cell of a = 12.5278(9) Å (Table S1 and Figure S1). The superstructure intensities in the (h,k,l=1.5) measured at 100 K are shown in Figure 1c which indicate a pseudo-cubic unit cell with a' = 2a. Figure S2 shows the 100 K (h,k,l=0.5) plane for the $MA_{0.5}FA_{0.5}PbI_3$ SC.

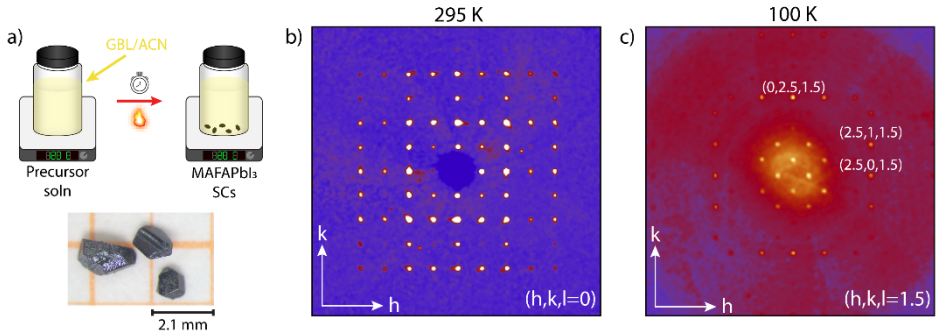

Figure 1: *a) Schematic of the ITC single crystal growth method with photograph of representative perovskite single crystals. b) Single crystal diffraction pattern along the (h,k,l=0) plane of $MA_{0.5}FA_{0.5}PbI_3$ collected at 295 K. c) Single crystal diffraction pattern along the (h,k,l=1.5) plane of $MA_{0.5}FA_{0.5}PbI_3$ collected at 100 K. The corresponding h and k axes are labeled for both patterns.*

Figure 2a supports the successful growth of the desired $MA_{0.5}FA_{0.5}PbI_3$ perovskite with a peak emission centered at ~800 nm, comparable to the report by Kim *et al.* for a similar composition.[41] To highlight the role of surface carrier recombination on the triplet generation process, two perovskite SCs with distinctly different PL decay dynamics are highlighted in following. The SC perovskite PL decays are fit to a triexponential function to capture the complex underlying dynamics in the first 1.5 µs:

$$I(t) = A_1 e^{-t/\tau_1} + A_2 e^{-t/\tau_2} + A_3 e^{-t/\tau_3}$$

The resulting lifetimes, amplitudes, and amplitude-weighted average lifetimes $\tau_{ave} = \frac{\sum A_i \tau_i}{\sum A_i}$ are tabulated in Table 1.

Table 1: Amplitudes (A), decay components (τ), and amplitude weighted lifetimes for the $MA_{0.5}FA_{0.5}PbI_3$ SCs based on a triexponential fitting.

	A_1	τ_1 (ns)	A_2	τ_2 (ns)	A_3	τ_3 (ns)	τ_{ave} (ns)	A_4	τ_4 (µs)
SC1	0.32	19.8	0.51	111	0.1	330	104	--	--
SC2	0.59	4.4	0.27	71	0.08	664	77	0.03	1.3

SC1 has a higher PL intensity (Figure 2a) than SC2. It also exhibits a relatively short PL lifetime, as it is fully decayed after 2 µs (τ_{ave} = 104 ns) (Figure 2b).[39] In contrast, SC2 has a lower PL intensity, which is in agreement with the observed rapid early-time component which can be attributed to rapid surface recombination, trapping, or diffusion of carriers away from the surface,[39,42] and a thus, a shorter amplitude-averaged carrier lifetime (τ_{ave} = 77 ns). However, after this 1.5 µs window, SC2 continues to decay with an additional monoexponential late-time component of τ_4 = 1.3 µs until it is fully decayed after 6 µs, indicating a low bulk trap density.

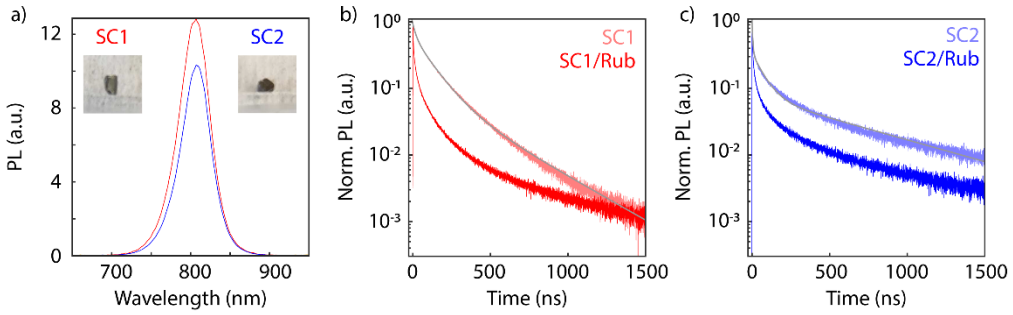

Figure 2: *a) Steady-state PL under 405 nm excitation at 29.6 W/cm^2 for SC1 and SC2 with images of each respective crystal. Normalized perovskite PL decay dynamics for SC1 (b) and SC2 (c) under an inert atmosphere (lighter color) and in a 19 mmol/L rubrene solution in chlorobenzene (darker color). Triexponential fits for the neat $MA_{0.5}FA_{0.5}PbI_3$ SC are included as light grey traces. The PL decays were taken under 780 nm excitation at 125 kHz and at a power density of 7.88 mW cm^{-2}.*

The same perovskite SCs were then placed in a 19 mmol/L (10 mg/mL) rubrene solution dissolved in chlorobenzene for studies of interfacial charge extraction resulting in UC.[9,29] Chlorobenzene is chosen as the solvent for rubrene since it is a common antisolvent for perovskite fabrication and our previous results indicate it minimally impacts the UC performance or the perovskite properties (compare Figure S3).[29] In both cases, early-time quenching of the PL decay dynamics indicates successful charge extraction at the perovskite surface, despite rubrene being present in solution and not as a solid-state layer as in previous studies.[9,43] Hence, charge transfer and subsequent triplet formation must occur rapidly during either a diffusion-based collision of rubrene and the perovskite SC, or the charge transfer process happens while rubrene briefly dynamically adsorbs to the surface of the SC. Our previous results indicate that triplets are

generated on a sub-nanosecond timescale[44] – a significantly shorter timescale than the expected time for adsorption/desorption and diffusion of rubrene in solution.

To ensure that the quenching of the perovskite PL results in spin-triplet states on rubrene and that TTA-UC occurs successfully, the emission spectrum is taken under 780 nm excitation. The resulting upconverted PL peaking at ~560 nm of the hybrid system is shown in Figure 3, highlighting the successful triplet sensitization in rubrene followed by TTA-UC.

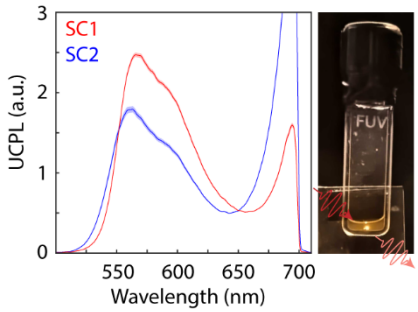

Figure 3: *Upconverted PL of $MA_{0.5}FA_{0.5}PbI_3$ SCs in rubrene taken under 780 nm excitation at 194 W cm^{-2}. Picture of successful upconverted PL from a $MA_{0.5}FA_{0.5}PbI_3$ SC in a 19 mmol/L rubrene solution under 780 nm excitation.*

The upconverted PL intensity in TTA-UC systems follows a unique power dependency: at low incident powers, triplets predominately decay through pathways other than the desired TTA-UC leading to a quadratic dependence of the PL intensity on the incident power.[45,46] Above the critical intensity threshold I_{th}, TTA-UC is the dominate triplet decay pathway and the UC process becomes efficient, and the power dependency reverts to linear. As a result, the intensity threshold can be found on a log-log plot of the upconverted power dependency *vs*. incident power as the intersection of a slope $\alpha = 2$ and $\alpha = 1$. However, the use of perovskite sensitizers complicates this relationship as the nonlinear dependence of the perovskite PL intensity I^{α} must be considered.[9,47–49] The power dependency of the perovskite PL is in the range of $1 < \alpha < 2$, due to the competition of mono molecular trap-assisted recombination and bimolecular non-geminate free-carrier recombination. Hence, the I_{th} describing the UC process is found at the crossing point of the slope ~2α and α.

The power dependency of the perovskite SC PL prior to the addition of rubrene and after the addition of rubrene are shown in Figure 4a,b for the previously described SC1 and SC2. The lower slope of SC1 compared to SC2 can be explained by an increased amount of monomolecular trap-assisted recombination in the more trap-rich perovskite SC1. The corresponding UC PL power dependence is depicted in Figure 4c,d. Clearly observable is that SC1 shows a distinct slope change from $\alpha = 3.6$ to $\alpha = 1.6$, leading to an $I_{th} = 1.05$ W cm^{-2}. SC2 on the other hand, experiences a lower $I_{th} = 331$ mW cm^{-2} due to a slope change from $\alpha = 2.4$ to $\alpha = 1.7$. Considering the slope of $\alpha = 2 \times 1.7$ is not reached, this can be seen as an upper bound for the I_{th}, or indicate disorder in the system, such that some regions are resulting in efficient UC, while others are still below the intensity threshold. Interestingly, we find overall brighter UC (at high power densities) for SC1 despite a higher intensity threshold. However, at low (solar-relevant) power densities below the intensity threshold, SC2 outperforms SC1. Comparing the results of several additional single crystals (Figures S4 and S5), we find no clear correlation between the I_{th} value and the overall UC intensity or the underlying perovskite PL intensity. A higher slope of the underlying perovskite PL intensity, however, can allow the UC PL intensity to increase more rapidly at higher incident powers, leading to comparable yields despite a higher *I*th value.

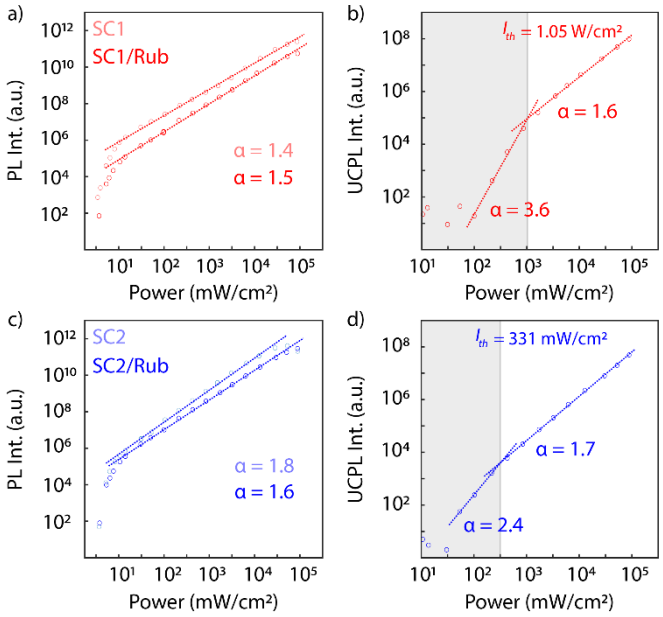

Figure 4: *a) Power-dependent perovskite PL intensity (>800 nm) for the SC1 under inert atmosphere (lighter color) and in the rubrene solution, (darker color). B) Power dependence of the upconverted emission intensity (610 – 680 nm) of SC1 fit with a slope change from α= 3.6 to α= 1.6 yields a threshold intensity, I_{th} = 1.05 W/cm^2. C) Power-dependent perovskite emission intensity for SC2 under inert atmosphere (lighter color) and in the rubrene solution (darker color). D) Upconverted emission intensity power dependence of SC2 with a slope change from α = 2.4 to α= 1.7 yields a threshold intensity, I_{th} = 331 mW/cm^2. All power dependent measurements were taken under 780 nm excitation.*

CONCLUSION

In conclusion, $MA_{0.5}FA_{0.5}PbI_3$ single crystals were successfully grown through a modified ITC process and structurally and optically characterized. Successful triplet generation at the perovskite SC/rubrene solution interface and subsequent TTA-UC in rubrene are demonstrated, yielding 560 nm emission under 780 nm excitation. Additional studies will be of interest to distinguish between a collision-based charge transfer and adsorption-based triplet generation mechanisms. In addition, further optimization of the hybrid system promises higher yields of TTA-UC. Importantly, this approach of hybrid UC at a mixed solid/liquid interface indicates that triplet states can be generated at the solid perovskite/liquid triplet acceptor interface for use in heterogeneous catalysis; enabling the decoupling of the solid-state triplet sensitizer and the reaction mixture. As a result, additional purification steps to remove the sensitizer from the reaction product will not be necessary. Future studies investigating triplet-based cross-coupling reactions will be of interest.

MATERIALS AND METHODS

Single Crystal Synthesis

Single Crystals of $MA_{0.5}FA_{0.5}PbI_3$ were prepared and grown using a solvent assisted inverse temperature crystallization method (ITC).[50] 1 M stock solutions of methylammonium lead triiodide ($MAPbI_3$) and formamidinium lead triiodide ($FAPbI_3$) were separately prepared in γ-butyrolactone (GBL). The solutions were then diluted to 0.5 M with acetonitrile (ACN) to fully dissolve the precursors. Equal volumes of $MAPbI_3$ and $FAPbI_3$ precursors in GBL/ACN were then combined into 4 mL vials and heated slowly until crystal formation began (~120 °C). Crystals were then removed from the solution and stored in an inert atmosphere (<0.5 ppm O_2 and H_2O).

Single Crystal X-Ray Diffraction

The SC-XRD measurement was carried out using an Oxford Diffraction Xcalibur-2 diffractometer equipped with a Sapphire2 detector and Mo K_α 0.71073 Å, where the sample was under continuous nitrogen flow at room temperature. The analysis of the scanned frames to identify the peaks and subsequently calculate the unit cell and symmetry was performed using the CrysAlisPro software.[51] The initial results of this analysis were used to determine the structure using Crystals software.[52]

Steady-State Optical Spectroscopy

For spectroscopy, $MA_{0.5}FA_{0.5}PbI_3$ SCs were placed into 300 μL cuvettes in an inert atmosphere for optical characterization. Following characterization of the SC under inert atmosphere, 25 μL of 19 mmol/L of rubrene in chlorobenzene (CB) was added to the cuvette.

Steady-state PL spectra were measured using an Ocean Insight emission spectrometer (HR2000+ES). A 405 nm continuous wave (CW) laser (PicoQuant LDH-D-C-405) connected to a PicoQuant laser driver (PDL 800-D) was used with a 650 nm long pass filter to measure the near-infrared perovskite PL. A 780 nm CW laser (PicoQuant LDH-D-C-780) connected to a PicoQuant laser driver (PDL 800-D) with a 700 nm short pass filter was used to measure the upconverted PL.

Time Resolved Photoluminescence Spectroscopy

Time-resolved photoluminescence (TRPL) decay dynamics were collected *via* time-correlated single-photon counting (TCSPC) using a pulsed 780 nm laser (PicoQuant LDH-D-C-780) at a repetition frequency of 125 kHz. A 780 nm notch filter was used to remove excess laser scatter. For perovskite decay dynamics, an 800 nm long pass filter was used in addition to the 780 nm notch filter. For power dependent PL intensity measurements, a 780 nm CW laser (PicoQuant LDH-D-C-780) was used, and the PL intensity was integrated for 20 s. In the TRPL and the power dependent measurements, the sample emission was focused onto a single photon counting avalanche diode (Micro Photon Devices) and photon arrival times were

recorded using a MultiHarp 150 event timer. The spot size for the 780 nm laser was determined using the razor blade method (90:10).

ASSOCIATED CONTENT

Supporting Information.

Scatter plot and table of the superstructure to substructure ratios. Single crystal diffraction pattern along the (h,k,l=0.5) plane. Optical characterization of additional single crystals.

AUTHOR INFORMATION

Corresponding Author

*E-mail: siegrist@magnet.fsu.edu and lnienhaus@fsu.edu

Data Availability

The raw data is available at DOI 10.17605/OSF.IO/QRJV3.

Notes

The authors declare no conflicts of interest.

Acknowledgements

G.M., C.M.S., A.P.C., and L.N. acknowledge funding by the National Science Foundation under Grant No. DMR-2237977 and the Camille and Henry Dreyfus Foundation (TC-23-050). M.M. and T.S. performed part of the work at the National High Magnetic Field Laboratory, which is supported by the National Science Foundation under grant DMR-1644779 and DMR- 2128556 and the State of Florida.

REFERENCES

(1) Alves, J.; Feng, J.; Nienhaus, L.; Schmidt, T. W. Challenges, Progress and Prospects in Solid State Triplet Fusion Upconversion. *J. Mater. Chem. C* **2022**, *10* (20), 7783–7798. https://doi.org/10.1039/D1TC05659J.

(2) VanOrman, Z. A.; Drozdick, H. K.; Wieghold, S.; Nienhaus, L. Bulk Halide Perovskites as Triplet Sensitizers: Progress and Prospects in Photon Upconversion. *J. Mater. Chem. C* **2021**, *9* (8), 2685–2694. https://doi.org/10.1039/D1TC00245G.

(3) Singh-Rachford, T. N.; Castellano, F. N. Photon Upconversion Based on Sensitized Triplet–Triplet Annihilation. *Coord. Chem. Rev.* **2010**, *254* (21), 2560–2573. https://doi.org/10.1016/j.ccr.2010.01.003.

(4) Schmidt, T. W.; Castellano, F. N. Photochemical Upconversion: The Primacy of Kinetics. *J. Phys. Chem. Lett.* **2014**, *5* (22), 4062–4072. https://doi.org/10.1021/jz501799m.

(5) Watthage, S. C.; Song, Z.; Phillips, A. B.; Heben, M. J. Chapter 3 - Evolution of Perovskite Solar Cells. In *Perovskite Photovoltaics*; Thomas, S., Thankappan, A., Eds.; Academic Press, 2018; pp 43–88. https://doi.org/10.1016/B978-0-12-812915-9.00003-4.

(6) Stoumpos, C. C.; Malliakas, C. D.; Peters, J. A.; Liu, Z.; Sebastian, M.; Im, J.; Chasapis, T. C.; Wibowo, A. C.; Chung, D. Y.; Freeman, A. J.; Wessels, B. W.; Kanatzidis, M. G. Crystal Growth of the Perovskite Semiconductor CsPbBr3: A New Material for High-Energy Radiation Detection. *Cryst. Growth Des.* **2013**, *13* (7), 2722–2727. https://doi.org/10.1021/cg400645t.

(7) Shang, Y.; Liao, Y.; Wei, Q.; Wang, Z.; Xiang, B.; Ke, Y.; Liu, W.; Ning, Z. Highly Stable Hybrid Perovskite Light-Emitting Diodes Based on Dion-Jacobson Structure. *Sci. Adv.* **2019**, *5* (8), eaaw8072. https://doi.org/10.1126/sciadv.aaw8072.

(8) Lee, M. M.; Teuscher, J.; Miyasaka, T.; Murakami, T. N.; Snaith, H. J. Efficient Hybrid Solar Cells Based on Meso-Superstructured Organometal Halide Perovskites. *Science* **2012**, *338* (6107), 643–647. https://doi.org/10.1126/science.1228604.

(9) Wieghold, S.; Bieber, A. S.; VanOrman, Z. A.; Daley, L.; Leger, M.; Correa-Baena, J.-P.; Nienhaus, L. Triplet Sensitization by Lead Halide Perovskite Thin Films for Efficient Solid-State Photon Upconversion at Subsolar Fluxes. *Matter* **2019**, *1* (3), 705–719. https://doi.org/10.1016/j.matt.2019.05.026.

(10) Kojima, A.; Teshima, K.; Shirai, Y.; Miyasaka, T. Organometal Halide Perovskites as Visible-Light Sensitizers for Photovoltaic Cells. *J. Am. Chem. Soc.* **2009**, *131* (17), 6050–6051. https://doi.org/10.1021/ja809598r.

(11) Min, H.; Lee, D. Y.; Kim, J.; Kim, G.; Lee, K. S.; Kim, J.; Paik, M. J.; Kim, Y. K.; Kim, K. S.; Kim, M. G.; Shin, T. J.; Il Seok, S. Perovskite Solar Cells with Atomically Coherent Interlayers on SnO2 Electrodes. *Nature* **2021**, *598* (7881), 444–450. https://doi.org/10.1038/s41586-021-03964-8.

(12) *Best Research-Cell Efficiency Chart*. https://www.nrel.gov/pv/cell-efficiency.html (accessed 2023-02-06).

(13) Das, B.; Liu, Z.; Aguilera, I.; Rau, U.; Kirchartz, T. Defect Tolerant Device Geometries for Lead-Halide Perovskites. *Mater. Adv.* **2021**, *2* (11), 3655–3670. https://doi.org/10.1039/D0MA00902D.

(14) Shi, D.; Adinolfi, V.; Comin, R.; Yuan, M.; Alarousu, E.; Buin, A.; Chen, Y.; Hoogland, S.; Rothenberger, A.; Katsiev, K.; Losovyj, Y.; Zhang, X.; Dowben, P. A.; Mohammed, O. F.; Sargent, E. H.; Bakr, O. M. Low Trap-State Density and Long Carrier Diffusion in Organolead Trihalide Perovskite Single Crystals. *Science* **2015**, *347* (6221), 519–522. https://doi.org/10.1126/science.aaa2725.

(15) Tao, S.; Schmidt, I.; Brocks, G.; Jiang, J.; Tranca, I.; Meerholz, K.; Olthof, S. Absolute Energy Level Positions in Tin- and Lead-Based Halide Perovskites. *Nat. Commun.* **2019**, *10* (1), 2560. https://doi.org/10.1038/s41467-019-10468-7.

(16) Beecher, A. N.; Semonin, O. E.; Skelton, J. M.; Frost, J. M.; Terban, M. W.; Zhai, H.; Alatas, A.; Owen, J. S.; Walsh, A.; Billinge, S. J. L. Direct Observation of Dynamic Symmetry Breaking above

Room Temperature in Methylammonium Lead Iodide Perovskite. *ACS Energy Lett.* **2016**, *1* (4), 880–887. https://doi.org/10.1021/acsenergylett.6b00381.
(17) Chen, Y.; He, M.; Peng, J.; Sun, Y.; Liang, Z. Structure and Growth Control of Organic–Inorganic Halide Perovskites for Optoelectronics: From Polycrystalline Films to Single Crystals. *Adv Sci* **2016**, *3*.
(18) Sullivan, C. M.; Nienhaus, L. Recharging Upconversion: Revealing Rubrene's Replacement. *Nanoscale* **2022**, *14* (46), 17254–17261. https://doi.org/10.1039/D2NR05309H.
(19) Sullivan, C. M.; Nienhaus, L. Generating Spin-Triplet States at the Bulk Perovskite/Organic Interface for Photon Upconversion. *Nanoscale* **2023**, *15* (3), 998–1013. https://doi.org/10.1039/D2NR05767K.
(20) Sullivan, C. M.; Nienhaus, L. Turning on TTA: Tuning the Energy Landscape by Intermolecular Coupling. *Chem. Mater.* **2023**. https://doi.org/10.1021/acs.chemmater.3c02349.
(21) Cheng, Y. Y.; Khoury, T.; Clady, R. G. C. R.; Tayebjee, M. J. Y.; Ekins-Daukes, N. J.; Crossley, M. J.; Schmidt, T. W. On the Efficiency Limit of Triplet–Triplet Annihilation for Photochemical Upconversion. *Phys. Chem. Chem. Phys.* **2010**, *12* (1), 66–71. https://doi.org/10.1039/B913243K.
(22) Singh-Rachford, T. N.; Castellano, F. N. Pd(II) Phthalocyanine-Sensitized Triplet−Triplet Annihilation from Rubrene. *J. Phys. Chem. A* **2008**, *112* (16), 3550–3556. https://doi.org/10.1021/jp7111878.
(23) Nienhaus, L.; Correa-Baena, J.-P.; Wieghold, S.; Einzinger, M.; Lin, T.-A.; Shulenberger, K. E.; Klein, N. D.; Wu, M.; Bulović, V.; Buonassisi, T.; Baldo, M. A.; Bawendi, M. G. Triplet-Sensitization by Lead Halide Perovskite Thin Films for Near-Infrared-to-Visible Upconversion. *ACS Energy Lett.* **2019**, 888–895. https://doi.org/10.1021/acsenergylett.9b00283.
(24) Wieghold, S.; Nienhaus, L. Precharging Photon Upconversion: Interfacial Interactions in Solution-Processed Perovskite Upconversion Devices. *J. Phys. Chem. Lett.* **2020**, *11* (3), 601–607. https://doi.org/10.1021/acs.jpclett.9b03596.
(25) Mase, K.; Okumura, K.; Yanai, N.; Kimizuka, N. Triplet Sensitization by Perovskite Nanocrystals for Photon Upconversion. *Chem. Commun.* **2017**, *53* (59), 8261–8264. https://doi.org/10.1039/C7CC03087H.
(26) Mongin, C.; Garakyaraghi, S.; Razgoniaeva, N.; Zamkov, M.; Castellano, F. N. Direct Observation of Triplet Energy Transfer from Semiconductor Nanocrystals. *Science* **2016**, *351* (6271), 369–372. https://doi.org/10.1126/science.aad6378.
(27) Wu, M.; Congreve, D. N.; Wilson, M. W. B.; Jean, J.; Geva, N.; Welborn, M.; Van Voorhis, T.; Bulović, V.; Bawendi, M. G.; Baldo, M. A. Solid-State Infrared-to-Visible Upconversion Sensitized by Colloidal Nanocrystals. *Nat. Photonics* **2016**, *10* (1), 31–34. https://doi.org/10.1038/nphoton.2015.226.
(28) Mahboub, M.; Huang, Z.; Tang, M. L. Efficient Infrared-to-Visible Upconversion with Subsolar Irradiance. *Nano Lett.* **2016**, *16* (11), 7169–7175. https://doi.org/10.1021/acs.nanolett.6b03503.
(29) Sullivan, C. M.; Bieber, A. S.; Drozdick, H. K.; Moller, G.; Kuszynski, J. E.; VanOrman, Z. A.; Wieghold, S.; Strouse, G. F.; Nienhaus, L. Surface Doping Boosts Triplet Generation Yield in Perovskite-Sensitized Upconversion. *Adv. Opt. Mater.* **2023**, *11* (1), 2201921. https://doi.org/10.1002/adom.202201921.
(30) Wang, L.; Yoo, J. J.; Lin, T.-A.; Perkinson, C. F.; Lu, Y.; Baldo, M. A.; Bawendi, M. G. Interfacial Trap-Assisted Triplet Generation in Lead Halide Perovskite Sensitized Solid-State Upconversion. *Adv. Mater.* **2021**, *33* (27), 2100854. https://doi.org/10.1002/adma.202100854.
(31) Adhyaksa, G. W. P.; Brittman, S.; Āboliņš, H.; Lof, A.; Li, X.; Keelor, J. D.; Luo, Y.; Duevski, T.; Heeren, R. M. A.; Ellis, S. R.; Fenning, D. P.; Garnett, E. C. Understanding Detrimental and Beneficial Grain Boundary Effects in Halide Perovskites. *Adv. Mater.* **2018**, *30* (52), 1804792. https://doi.org/10.1002/adma.201804792.
(32) Wieghold, S.; Bieber, A. S.; VanOrman, Z. A.; Rodriguez, A.; Nienhaus, L. Is Disorder Beneficial in Perovskite-Sensitized Solid-State Upconversion? Role of DBP Doping in Rubrene. *J. Phys. Chem. C* **2020**, *124* (33), 18132–18140. https://doi.org/10.1021/acs.jpcc.0c05290.

(33) Bossanyi, D. G.; Sasaki, Y.; Wang, S.; Chekulaev, D.; Kimizuka, N.; Yanai, N.; Clark, J. In Optimized Rubrene-Based Nanoparticle Blends for Photon Upconversion, Singlet Energy Collection Outcompetes Triplet-Pair Separation, Not Singlet Fission. *J. Mater. Chem. C* **2021**. https://doi.org/10.1039/D1TC02955J.
(34) Breen, I.; Tempelaar, R.; Bizimana, L. A.; Kloss, B.; Reichman, D. R.; Turner, D. B. Triplet Separation Drives Singlet Fission after Femtosecond Correlated Triplet Pair Production in Rubrene. *J. Am. Chem. Soc.* **2017**, *139* (34), 11745–11751. https://doi.org/10.1021/jacs.7b02621.
(35) Jiang, Y.; Weiss, E. A. Colloidal Quantum Dots as Photocatalysts for Triplet Excited State Reactions of Organic Molecules. *J. Am. Chem. Soc.* **2020**, *142* (36), 15219–15229. https://doi.org/10.1021/jacs.0c07421.
(36) Alonso, R.; Bach, T. A Chiral Thioxanthone as an Organocatalyst for Enantioselective [2+2] Photocycloaddition Reactions Induced by Visible Light. *Angew. Chem. Int. Ed.* **2014**, *53* (17), 4368–4371. https://doi.org/10.1002/anie.201310997.
(37) Weiss, R.; VanOrman, Z. A.; Sullivan, C. M.; Nienhaus, L. A Sensitizer of Purpose: Generating Triplet Excitons with Semiconductor Nanocrystals. *ACS Mater. Au* **2022**, *2* (6), 641–654. https://doi.org/10.1021/acsmaterialsau.2c00047.
(38) Saidaminov, M. I.; Abdelhady, A. L.; Murali, B.; Alarousu, E.; Burlakov, V. M.; Peng, W.; Dursun, I.; Wang, L.; He, Y.; Maculan, G.; Goriely, A.; Wu, T.; Mohammed, O. F.; Bakr, O. M. High-Quality Bulk Hybrid Perovskite Single Crystals within Minutes by Inverse Temperature Crystallization. *Nat. Commun.* **2015**, *6* (1), 7586. https://doi.org/10.1038/ncomms8586.
(39) Nayak, P. K.; Moore, D. T.; Wenger, B.; Nayak, S.; Haghighirad, A. A.; Fineberg, A.; Noel, N. K.; Reid, O. G.; Rumbles, G.; Kukura, P.; Vincent, K. A.; Snaith, H. J. Mechanism for Rapid Growth of Organic–Inorganic Halide Perovskite Crystals. *Nat. Commun.* **2016**, *7* (1), 13303. https://doi.org/10.1038/ncomms13303.
(40) Breternitz, J.; Tovar, M.; Schorr, S. Twinning in MAPbI3 at Room Temperature Uncovered through Laue Neutron Diffraction. *Sci. Rep.* **2020**, *10* (1), 16613. https://doi.org/10.1038/s41598-020-73487-1.
(41) Kim, H.; Byun, H. R.; Jeong, M. S. Synthesis and Characterization of Multiple-Cation Rb(MAFA)PbI3 Perovskite Single Crystals. *Sci. Rep.* **2019**, *9* (1), 2022. https://doi.org/10.1038/s41598-019-38947-3.
(42) Wenger, B.; Nayak, P. K.; Wen, X.; Kesava, S. V.; Noel, N. K.; Snaith, H. J. Consolidation of the Optoelectronic Properties of CH3NH3PbBr3 Perovskite Single Crystals. *Nat. Commun.* **2017**, *8* (1), 590. https://doi.org/10.1038/s41467-017-00567-8.
(43) Wieghold, S.; Bieber, A. S.; VanOrman, Z. A.; Nienhaus, L. Influence of Triplet Diffusion on Lead Halide Perovskite-Sensitized Solid-State Upconversion. *J. Phys. Chem. Lett.* **2019**, 3806–3811. https://doi.org/10.1021/acs.jpclett.9b01526.
(44) Conti, C. R.; Bieber, A. S.; VanOrman, Z. A.; Moller, G.; Wieghold, S.; Schaller, R. D.; Strouse, G. F.; Nienhaus, L. Ultrafast Triplet Generation at the Lead Halide Perovskite/Rubrene Interface. *ACS Energy Lett.* **2022**, *7* (2), 617–623. https://doi.org/10.1021/acsenergylett.1c02732.
(45) Monguzzi, A.; Mezyk, J.; Scotognella, F.; Tubino, R.; Meinardi, F. Upconversion-Induced Fluorescence in Multicomponent Systems: Steady-State Excitation Power Threshold. *Phys. Rev. B* **2008**, *78* (19), 195112. https://doi.org/10.1103/PhysRevB.78.195112.
(46) Ronchi, A.; Monguzzi, A. Developing Solid-State Photon Upconverters Based on Sensitized Triplet–Triplet Annihilation. *J. Appl. Phys.* **2021**, *129* (5), 050901. https://doi.org/10.1063/5.0034943.
(47) Richter, J. M.; Abdi-Jalebi, M.; Sadhanala, A.; Tabachnyk, M.; Rivett, J. P. H.; Pazos-Outón, L. M.; Gödel, K. C.; Price, M.; Deschler, F.; Friend, R. H. Enhancing Photoluminescence Yields in Lead Halide Perovskites by Photon Recycling and Light Out-Coupling. *Nat. Commun.* **2016**, *7*, 13941. https://doi.org/10.1038/ncomms13941.
(48) Stranks, S. D.; Burlakov, V. M.; Leijtens, T.; Ball, J. M.; Goriely, A.; Snaith, H. J. Recombination Kinetics in Organic-Inorganic Perovskites: Excitons, Free Charge, and Subgap States. *Phys. Rev. Appl.* **2014**, *2* (3), 034007. https://doi.org/10.1103/PhysRevApplied.2.034007.

(49) Sum, T. C.; Mathews, N. Advancements in Perovskite Solar Cells: Photophysics behind the Photovoltaics. *Energy Environ. Sci.* **2014**, *7* (8), 2518–2534. https://doi.org/10.1039/C4EE00673A.
(50) Ku, Z.; Tiep, N. H.; Wu, B.; Sum, T. C.; Fichou, D.; Fan, H. J. Solvent Engineering for Fast Growth of Centimetric High-Quality CH3NH3PbI3 Perovskite Single Crystals. *New J. Chem.* **2016**, *40* (9), 7261–7264. https://doi.org/10.1039/C6NJ00188B.
(51) CrysAlisPRO.
(52) Betteridge, P. W.; Carruthers, J. R.; Cooper, R. I.; Prout, K.; Watkin, D. J. CRYSTALS Version 12: Software for Guided Crystal Structure Analysis. *J. Appl. Crystallogr.* **2003**, *36* (6), 1487–1487. https://doi.org/10.1107/S0021889803021800.

TOC Graphic